Accurate Parabolic Navier-Stokes solutions of the supersonic flow around an elliptic cone

Pedro Paredes* and Vassilis Theofilis†

School of Aeronautics, Universidad Politécnica de Madrid, E-28040 Madrid, Spain

Flows of relevance to new generation aerospace vehicles exist, which are weakly dependent on the streamwise direction and strongly dependent on the other two spatial directions, such as the flow around the (flattened) nose of the vehicle and the associated elliptic cone model. Exploiting these characteristics, a parabolic integration of the Navier-Stokes equations is more appropriate than solution of the full equations, resulting in the so-called Parabolic Navier-Stokes (PNS). This approach not only is the best candidate, in terms of computational efficiency and accuracy, for the computation of steady base flows with the appointed properties, but also permits performing instability analysis and laminar-turbulent transition studies a-posteriori to the base flow computation. This is to be contrasted with the alternative approach of using order-of-magnitude more expensive spatial Direct Numerical Simulations (DNS) for the description of the transition process. The PNS equations used here have been formulated for an arbitrary coordinate transformation and the spatial discretization is performed using a novel stable high-order finite-difference-based numerical scheme, ensuring the recovery of highly accurate solutions using modest computing resources. For verification purposes, the boundary layer solution around a circular cone at zero angle of attack is compared in the incompressible limit with theoretical profiles. Also, the recovered shock wave angle at supersonic conditions is compared with theoretical predictions in the same circular-base cone geometry. Finally, the entire flow field, including shock position and compressible boundary layer around a 2:1 elliptic cone is recovered at Mach numbers 3 and 4.

Nomenclature

Abbreviations

DNS	Direct Numerical Simulations
FD-q	Stable high-order Finite Differences of order q
PDE	Partially Differential Equations
PNS	Parabolic Navier-Stokes equations

Latin Symbols

(x, y, z)	Cartesian coordinates
$\mathbf{q}$	Flow vector

Greek Symbols

(ξ, η, ζ)	Curvilinear coordinates
α	Cone half angle
β	Shock wave angle

Superscript

*Student Member AIAA. Correspondence to: pedro.paredes@upm.es
†Research Professor, Associate Fellow AIAA

* Dimensional quantities

I. Introduction

Prediction of laminar-turbulent flow transition and the associated heat-transfer in high-speed flows, as well as control of both phenomena, is key in optimizing performance of next-generation aerospace vehicles. The elliptic cone is a frequently used model to understand transition over components of such vehicles. Evidence has been accumulated regarding laminar-turbulent transition scenarios on elliptic cones at aspect ratios 2:1 and 4:1, exposed at zero angle of attack to oncoming flows for Mach numbers (M) between 4 and 8 in different experimental facilities,[1–4] while recently large-scale computations of the same phenomenon have appeared in the literature.[5] All these studies reported the formation of large structures near the minor-axis centerline of the cone; these structures were first experimentally found by Schmisseur *et al.*[1,2] to be most receptive to amplification of perturbations in a 4:1 elliptic cone at $M = 4$. Simultaneously, Poggie & Kimmel[3] reported evidence of the classical crossflow and second Mack mode instabilities in a 2:1 elliptic cone at $M = 8$; the transition front was asymmetric, with early transition near the top centerline and delayed transition near the leading edge. Images taken by Huntley & Smits[4] of the early stages of transition, on a sharp-nosed 4:1 elliptic cone at same Ma, confirm that transition begins with the emergence of small-scale structures near the centerline axis of the cone, rather than in the outboard cross-flow region. Recent large-scale computations by Bartkowicz *et al.*[5] confirm the co-existence of all these scenarios and attempt a first classification of their significance at different Reynolds number (Re) range: while the centerline structures lead flow to transition at lower Re values, crossflow instability near the elliptic cone leading edge becomes competitive at higher Reynolds numbers. The origin and role of the large centerline structures in the laminar-turbulent transition process on the elliptic cone is presently unclear. Mapping of the parameter space with respect to critical conditions and study of nonlinear interactions of different modal scenarios potentially leading flow to transition are issues hardly to be addressed by large-scale computations; instability theory is the natural tool to accomplish these tasks.

It is well-known that instability analysis results are strongly dependent on the details of the base flow. Small differences in the base flow can lead to remarkable differences in the predicted amplifications, due to the exponential nature of linear modal instability. The recovery of accurate base flows using direct numerical simulations (DNS) in circumstances in which the flow is steady *per se* -and thus, stable-, or along with a Newton-iteration technique[6] in cases in which an unsteady flow would exist, though feasible, may require large computational resources for three-dimensional flows. On the other hand, there exists a class of flows in which a predominant direction exists, along which the mean properties of the flow field vary slowly, while fast variations occur on the cross-sectional planes. Examples of these flows are corner flows, square- or serrated-nozzle jets, missile-shaped bodies -elliptic cones- or systems of trailing-vortices in wakes. The geometrical particularities of this kind of flows can be exploited in order to devise *ad hoc* approaches for the computation of base flows, that are inherently more efficient than use of DNS. The same premises can be invoked in order to perform subsequent instability analyses of these flows using three-dimensional Parabolized Stability Equations (PSE-3D).[7,8] This base flow computation methodology is a three-dimensional extension of multiple-scale instability analysis terms of Bouthier[9] and Gaster,[10] formulated as Parabolized Stability Equations two decades later;[11,12] see Herbert[13] for a review.

The present work presents an algorithm for the accurate and efficient computation of this class of base flows, based on the Parabolic Navier-Stokes (PNS) equations.[14] Since their appearance, the PNS equations have been used to successfully compute three-dimensional, mostly supersonic/hypersonic, viscous flows; see[15,16] for a review. One of the advantages of using PNS for the computation of base flows in an instability analysis context, is the steadiness of its solutions by definition. In this manner, fluctuations occurring in the real flow will be recovered as instabilities of the flow, in the subsequent instability analysis.

The first PNS calculations of three-dimensional viscous flows over cone-based shaped bodies at nonzero Angle of Attack (AoA) was presented by Lin & Rubin,[17,18] where the authors computed the boundary later over a slender cone at moderate incidence (ratio between AoA and half-cone vertex angle is lower or equal than 2). The same authors also published the PNS calculations on spinning cones at nonzero AoA.[19] Almost contemporary, Helliwell & Lubard[20,21] developed their PNS code and showed calculations over a circular cone at high AoA. In the next decade, Tannehill *et al.*[22] developed a general PNS code to compute the steady supersonic viscous flow around arbitrary body shapes at high AoA and used it to calculate the

laminar flow over a slab delta wing with 70^0 sweep at AoA up to 41.5^0 and Ma equal to 6.8 and 9.6. Some years later, Lawrence *et al.*[23] showed PNS calculations for two body shapes: a circular cone of 10^0 half-angle at $AoA = 12^0$, 20^0 and 24^0 and an elliptic cone-based all-body hypersonic vehicle at $AoA = 0^0$ and 10^0, which can be considered as the first PNS calculation of the viscous flow over an elliptic cone. Motivated by the NASP effort in the early 90s, Stuckert& Reed[24] presented PNS base flow computations and local modal stability analysis of hypersonic, chemically reacting, viscous flow over a circular cone at zero AoA. The supersonic and hypersonic PNS calculations research of the three-dimensional boundary-layer over elliptic cross-section cones was undertaken by Lyttle & Reed,[25] who presented solutions for adiabatic wall elliptic cones of eccentricities of 2:1, 3:1 and 4:1 at $M = 4$, applying Reynolds number correlations based on the parameter R (see Reed & Haynes[26]) for stability analysis. The parameter R for these configurations peaked near the top centerline, outside the region of validity of the above correlation. Boundary layer velocity profiles near the top centerline were inflectional and unstable. Kimmel *et al.*[27] used an extended version of the the UPS PNS code,[28,29] enabling the study of cool-wall cases, for computing the base flow around cones with eccentricities of 1.5:1, 2:1 and 4:1 at $M = 7.95$. The e^{Malik} code[30] was used to calculate boundary layer stability, demonstrating that all the three cases showed crossflow instability, with the 4:1 configuration attaining the highest N factors. A further study for a wide range of AoA, Ma, Re and eccentricities is the scope of the present work, starting from the computation of the accurate steady base flows using a newly-developed PNS code with state-of-the-art techniques.

In the present work, the PNS equations are derived from the compressible three-dimensional Navier-Stokes equations written in a generalized coordinate system by assuming stationarity and neglecting only the viscous streamwise second order derivative terms. Doing this, the equations change their mathematical nature, from elliptic to parabolic, and a parabolic integration along the streamwise direction is permissible. The numerical solution of the problem for flows of practical application is challenging, as it involves the inversion of large matrices, resulting form the discretization of a system of two-dimensional partial derivative equations, with leading dimension $\mathcal{O}(10^4 - 10^5)$. The challenge is met by use of stable high-order finite-differences schemes, developed recently by Hermanns and Hernández,[31] together with the parallelizable sparse matrix linear algebra package MUMPS.[32,33] This combination exploits the high level of sparsity pattern offered by the finite-difference spatial differentiation, improving substantially the numerical efficiency while keeping accuracy. In the recent work of Paredes *et al.*,[34] a thorough study of global stability problems using this high-order finite differences of order q (FD-q) and sparse matrix inversion, permitted resolution of the PDE-based eigenvalue problems on typical desktop computers, as opposed to supercomputing facilities necessary when spectral methods are used at the same level of accuracy.[35]

The PNS equations are formulated in a general coordinate system for compressible flows in Section II. The numerical solution procedure of the PNS equations is presented in Section III. Section IV shows verifications and validations of the newly-developed code, whose are carried out solving the flow around a circular cone at zero AoA. Solutions of the supersonic flow around a 7^0 half minor-axis angle 2:1 elliptic cone at Mach numbers 3 and 4 are presented in same Section. Summary and concluding remarks are offered in Section V.

II. Parabolic Navier-Stokes equations

The Parabolic Navier-Stokes (PNS) equations are derived from the three-dimensional steady Navier-Stokes equations, whose are

$$\nabla \cdot (\rho^* \mathbf{V}^*) = 0, \tag{1}$$

$$\rho^* (\mathbf{V}^* \cdot \nabla)\mathbf{V}^* = -\nabla p^* + \nabla[\lambda^* (\nabla \cdot \mathbf{V}^*)] + \nabla \cdot [\mu^* ((\nabla \mathbf{V}^*) + (\nabla \mathbf{V}^*)^{\mathbf{T}})], \tag{2}$$

$$\rho^* c_v^* [(\mathbf{V}^* \cdot \nabla)\mathbf{T}^*] = -p^* \nabla \cdot \mathbf{V}^* + \nabla \cdot (\kappa^* \nabla \mathbf{T}^*) + \lambda^* (\nabla \cdot \mathbf{V}^*)^{\mathbf{2}} + \frac{\mu^*}{\mathbf{2}} [(\nabla \mathbf{V}^*) + (\nabla \mathbf{V}^*)^{\mathbf{T}}]^{\mathbf{2}}, \tag{3}$$

where $\mathbf{V}^*$ is the velocity vector, ρ^* the density, p^* the pressure, T^* the temperature, c_p^* the specific heat, κ^* the thermal conductivity, μ^* the first coefficient of viscosity, and λ^* the second coefficient of viscosity. Note that using the Stoke's law $\lambda^* = -2/3\mu^*$. The equation of state is given by the perfect gas relation $p^* = \rho^* \mathcal{R} T^*$.

The non-dimensionalization of above equations is carried out as follows. The lengths are scaled by a reference length L^*, velocity by U_e^* and temperature by T_e^*. The reference pressure is $p_e^* = \rho_e^* (U_e^*)^2$, the

free-stream sound speed is denoted by s_e^*, and $\gamma = c_{p,e}^*/c_{v,e}^*$. The resulting non-dimensional parameters are the Reynolds number, $Re = \rho_e^* U_e^* L/\mu_e^*$, the Prandtl number $Pr = c_{p,e}^* \mu_e^*/\kappa_e^*$, the Mach number $M = U_e^*/s_e^*$ and the Eckert number $Ec = (U_e^*)^2/(c_{p,e}^* T_e^*) = (\gamma - 1)M^2$. The non-dimensionalized equation of state for ideal gas is

$$p = \frac{1}{\gamma M^2}\rho T, \tag{4}$$

where the constant of perfect gases is fixed to $\gamma = 1.4$ and the Prandtl number $Pr = 0.72$. The Sutherland's law is used for the viscosity coefficient

$$\mu = (T)^{3/2}\frac{1+S}{T+S}, \tag{5}$$

setting $S = 110.4\ K/T_e^*$.

A general coordinate transformation of the form

$$\xi = \xi(x), \qquad \eta = \eta(x,y,z), \qquad \zeta = \zeta(x,y,z), \tag{6}$$

is used to transform the governing equations into the (ξ, η, ζ) system. This transformation restricts the (η, ζ) solution surfaces to be in a plane normal to the x axis. Using the chain rule of partial differentiation, the first order partial derivatives become

$$\frac{\partial}{\partial x} = \xi_x\frac{\partial}{\partial \xi} + \eta_x\frac{\partial}{\partial \eta} + \zeta_x\frac{\partial}{\partial \zeta}, \qquad \frac{\partial}{\partial y} = \eta_y\frac{\partial}{\partial \eta} + \zeta_y\frac{\partial}{\partial \zeta}, \qquad \frac{\partial}{\partial z} = \eta_z\frac{\partial}{\partial \eta} + \zeta_z\frac{\partial}{\partial \zeta}, \tag{7}$$

Note that $\xi_y = \xi_z = 0$. The metrics $(\xi_x, \eta_x, \eta_y, \eta_z, \zeta_x, \zeta_y, \zeta_z)$ appearing in these equations are determined using

$$\begin{pmatrix} \xi_x & 0 & 0 \\ \eta_x & \eta_y & \eta_z \\ \zeta_x & \zeta_y & \zeta_z \end{pmatrix} = \begin{pmatrix} x_\xi & 0 & 0 \\ y_\xi & y_\eta & y_\zeta \\ z_\xi & z_\eta & z_\zeta \end{pmatrix}^{-1} = J\begin{pmatrix} y_\eta z_\zeta - y_\zeta z_\eta & 0 & 0 \\ -(y_\xi z_\zeta - y_\zeta z_\xi) & x_\xi z_\zeta & -x_\xi y_\zeta \\ y_\xi z_\eta - y_\eta z_\xi & x_\xi z_\eta & x_\xi y_\eta \end{pmatrix}, \tag{8}$$

where J is the Jacobian of the transformation, which can be evaluated in the following manner

$$J = \frac{\partial(\xi,\eta,\zeta)}{\partial(x,y,z)} = 1/J^{-1} = 1\Big/\frac{\partial(x,y,z)}{\partial(\xi,\eta,\zeta)} = 1\Big/\begin{vmatrix} x_\xi & 0 & 0 \\ y_\xi & y_\eta & y_\zeta \\ z_\xi & z_\eta & z_\zeta \end{vmatrix} = 1/\left[x_\xi(y_\eta z_\zeta - y_\zeta z_\eta)\right]. \tag{9}$$

In order to express second order derivatives in terms of computational coordinate derivatives, the next equivalence, written using Einstein notation, is used:

$$\frac{\partial f}{\partial x_i} = \xi_{x_i}^j\frac{\partial f}{\partial \xi^j} = J\frac{\partial}{\partial \xi^j}\left(\frac{\xi_{x_i}^j f}{J}\right) - Jf\left[\frac{\partial}{\partial \xi^j}\left(\frac{\xi_{x_i}^j}{J}\right)\right], \tag{10}$$

where $f = f(x,y,z)$ is an arbitrary scalar function, $i = 1,2,3$, $j = 1,2,3$, $(x_1, x_2, x_3) = (x, y, z)$ and $(\xi^1, \xi^2, \xi^3) = (\xi, \eta, \zeta)$. The term in square brackets is equal to zero. This can be verified by substituting the metrics given by Eq. (8) into this term. Then, using the above expression (10), the second order derivative with respect to the physical coordinates x_i and x_j of an arbitrary scalar function f is expressed as follow

$$\frac{\partial^2 f}{\partial x_i \partial x_j} = \xi_{x_i}^k\frac{\partial}{\partial \xi^k}\left(\xi_{x_j}^l\frac{\partial f}{\partial \xi^l}\right) = J\frac{\partial}{\partial \xi^k}\left(\frac{\xi_{x_i}^k \xi_{x_j}^l \frac{\partial f}{\partial \xi^l}}{J}\right) = \xi_{x_i}^k\xi_{x_j}^l\frac{\partial^2 f}{\partial \xi^k \partial \xi^l} + J\frac{\partial}{\partial \xi^k}\left(\frac{\xi_{x_i}^k \xi_{x_j}^l}{J}\right)\frac{\partial f}{\partial \xi^l}. \tag{11}$$

The derivation of the Parabolic Navier-Stokes (PNS) equations from the three-dimensional steady Navier-Stokes equations (1)-(3) is valid in the limit of large Reynolds number when the flow configuration is predominant along the streamwise direction and exhibits a slow spatial dependence in the same direction, ξ. Therefore, the streamwise viscous derivative terms are negligible compared to the normal and transverse viscous derivative terms:

$$L_\xi \gg L_\eta, L_\zeta, \quad \partial(\,)/\partial\xi \ll \partial(\,)/\partial\eta, \partial(\,)/\partial\zeta, \quad \partial(\,)^2/\partial^2\xi \lll \partial(\,)^2/\partial^2\eta, \partial(\,)^2/\partial^2\zeta, \tag{12}$$

where L_ξ, L_η and L_ζ are the characteristic lengths on the streamwise and normal to it spatial directions respectively. Hence the PNS equations are derived here by simply dropping second order partial derivatives with respect to the streamwise direction from the steady Navier-Stokes equations (1)-(3).[16] When there is no flow, or reversed flow along the slow direction, the downstream integration of the Navier-Stokes equations is not correct, and numerical instabilities will prevent the recovery of converged solutions.

The parabolization of equations is not totally correct due to the term p_ξ, which is associated with the left-running characteristic (for subsonic flows only) allowing upstream influence. The technique for handling the pressure gradient term was proposed by Vigneron *et al.*[36] In this approach, the upstream propagation is suppressed by multiplying the streamwise pressure gradient p_ξ by a parameter Ω given by

$$\Omega = \begin{cases} \frac{\gamma M_\xi^2}{1+(\gamma-1)M_\xi^2}, & M_\xi < 1 \\ 1, & M_\xi \geq 1 \end{cases} \tag{13}$$

III. Numerical considerations

A. Transformations

Different coordinate transformations are needed to transform the computational domain system (ξ, η, ζ) into the desired physical coordinate system (x, y, z).

1. *Circular cone*

The mesh surrounding a circular cone is calculated using a modification of the cylindrical transformation, written as

$$x = \xi, \qquad y = (\xi \tan\alpha + \eta\eta_\infty)\sin\zeta, \qquad z = (\xi \tan\alpha + \eta\eta_\infty)\cos\zeta, \tag{14}$$

where $\eta \in [0, 1]$ and η_∞ controls the farfield boundary.

2. *Elliptic cone*

For the elliptic cone problem, a modified confocal elliptic transformation is used,

$$x = \xi, \qquad y = c\xi \sinh(\eta_0 + \eta\eta_\infty)\sin\zeta, \qquad z = c\xi \cosh(\eta_0 + \eta\eta_\infty)\cos\zeta, \tag{15}$$

where c sets the half angle of the cone minor-axis, $c = \text{atan}\alpha/\sinh\eta_0$, and η_0 is a parameter controlling the Aspect Ratio (AR) of the cone, $\eta_0 = \text{atanh}\,(1/AR)$.

B. Spatial discretization

The spatial discretization in ξ is performed using Backward Differentiation Formulas (BDF). The BDF have the following general form for a k-step method

$$\frac{\partial \mathbf{q}_m}{\partial \xi} = \Delta\xi \sum_{i=0}^{k} a_i \mathbf{q}_{m-i}, \tag{16}$$

where $\mathbf{q}_m = \mathbf{q}(\xi_m)$ and a_i are the scheme's coefficients. The one-step BDF is equivalent to the backward Euler method, $a_0 = 1$ and $a_1 = -1$.

The two directions of the normal plane to the streamwise marching direction, (η, ζ), are discretized using the stable high-order finite-differences numerical schemes of order q (FD-q) recently developed by Hermanns and Hernández.[31] These methods are used because of spectral-like accuracy is recovered, outperforming spectral collocation methods for stability analysis calculations in terms of accuracy and computational efficiency; see Paredes *et al.*[34]) for more details.

C. Non-linear marching integration

The derivation of the PNS equations implies a change in the mathematical nature of the steady Navier-Stokes equations, from elliptic to parabolic, and a marching integration on the streamwise direction is permissible.

The resulting discretized PNS equations are a system of nonlinear PDE. In order to solve the system, a marching integration along ξ is used together with Newton iteration method for solving the non-linear implicit scheme. A linear system is solved for update the solution in each ξ-station

$$\mathcal{J}(\mathbf{q}^{n-1})\Delta\mathbf{q} = \mathcal{F}_{\mathbf{q}}(\mathbf{q}^{n-1})\Delta\mathbf{q} = -\mathcal{F}(\mathbf{q}^n - 1), \tag{17}$$

where $\mathbf{q} = (\rho, u, v, w, T)^T$ is the fluid variables vector, $\mathcal{J} = \mathcal{F}_{\mathbf{q}}$ is the Jacobian of the operator $\mathcal{F}$, $\Delta\mathbf{q} = (\Delta\rho, \Delta u, \Delta v, \Delta w, \Delta T)^T$ and $\mathbf{q}^n = \mathbf{q}^{n-1} + \Delta\mathbf{q}$.

The inversion of the matrix discretizing the Jacobian operator $\mathcal{J}$, which leading dimension is $\mathcal{O}(10^4 - 10^5)$, is performed using the parallelizable sparse matrix linear algebra package MUMPS[32,33] and the SPARSKIT2 library.[37] These libraries exploit the high level of sparsity pattern offered by the finite-difference spatial differentiation, improving substantially on numerical efficiency while keeping accuracy; see the work of Paredes *et al.*[34] for more details.

The PNS marching scheme (17) has to be complemented with appropriate boundary conditions depending on the problem. For the cases studied here, the flow around a circular cone and around an elliptic cone, the symmetries of the problem are exploited for reducing computational requirements and the boundary conditions are imposed for the azimuthal direction, ζ. No-slip conditions are imposed at the wall, $\eta = 0$, together with Neumann conditions for temperature and density, which implies having adiabatic wall. At the farfield, $\eta = 1$, free-stream conditions are imposed. Note that with this boundary condition at the upper boundary of η, the shock wave is immersed in the domain.

The marching integration needs to be feed by an initial condition. Free-stream conditions, $\mathbf{q}_\infty = (\rho_\infty, u_\infty, v_\infty, w_\infty, T_\infty)^T$, i.e. $\mathbf{q}_\infty = (1, 1, 0, 0, 1)^T$ for AoA=0^0, are imposed at the vertex of the cone and the solution at an initial station ξ_0 is converged after some Newton iterations.

IV. Results

This Section firstly presents validations of the newly-developed code solving the boundary layer around a circular cone in the incompressible and compressible regimes. Secondly, the supersonic flow solutions around a 2:1 elliptic cone at Mach numbers 3 and 4 are presented.

A. Circular cone

The flow around a circular cone is well understood thanks to the axisymmetric condition, in which the streamlines remain in meridian planes. The boundary layer equations under rotational symmetry were first given by Mangler[38] in the incompressible limit, introducing the Mangler transformation, which converts the well-known Falker-Skan boundary layer solutions into the ones around circular cones. Figure 1(a) shows the streamwise velocity profiles for a circular cone with half angle $\alpha = 15^0$ setting $M = 10^{-3}$ and $Re = 100$ comparing with Mangler theory[38] at three different streamwise positions, $x = 100$, 200 and 300. Excellent agreement is observed, having an overlapping of both profiles.

In the theory of inviscid supersonic flow past a circular-based cone at zero incidence (see Shapiro[39] for more details), for $M > 1.2$ and a half cone angle less than 55^0, the resulting shock wave is attached to the cone vertex, and the flow at the cone surface is at constant velocity, pressure, and temperature. These properties base the analysis of Taylor and Maccoll,[40] in which the shock angle β is predicted versus the Mach number and half cone angle α. Figure 1(b) shows the comparisons between the PNS results and the inviscid theory predictions for Mach numbers 2 and 3. Excellent agreement is again observed.

B. Elliptic cone

In the elliptic cone problem, the three-dimensionality of the flow makes it unaffordable from an analytical point of view and more complex numerical tools are needed to recover the flow field. The three-dimensionality of the flow inevitable produces spanwise pressure gradients, which induce crossflow, at locations where the flow direction of the interior of the boundary layer is no longer co-planar with the edge velocity vector. This phenomenon causes the appearance of two main regions in the elliptic cone flow, the attachment line on the leading edge, i.e. the major-axis, and the top centerline, i.e. the minor-axis, where a lift-up process is observed.

The supersonic flow around a 7^0 half minor-axis angle angle 2:1 elliptic cone is solved at Mach numbers 3 and 4. Figures 2 and 3 show the iso-contours of the flow field variables from $Re_x = 10^4$ to $Re_x = 3 \times 10^4$.

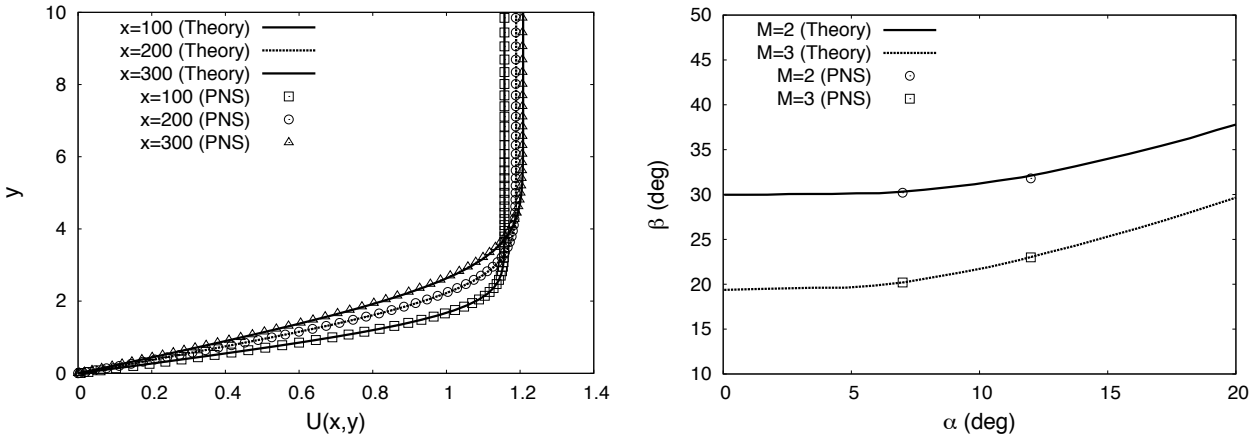

(a) (b)

Figure 1. Comparisons of theoretical predictions and results delivered by the newly-developed PNS code. Figure 1(a) shows the streamwise velocity profiles in a circular cone with half angle $\alpha = 15^0$ setting $M = 10^{-3}$ comparing with Mangler theory[38] at different streamwise positions. Figure 1(b) shows the shock angle β versus the half cone angle α for Mach numbers 2 and 3 comparing with the Taylor and Maccoll theoretical predictions[40].

The shock wave layer is clearly visible in the density plots 3(c) and 3(d). The crossflow region is observed in Figures 2(e) and 2(f), near the wall of the cone, where $w < 0$. Figure 4 shows some streamlines near the wall for the $M = 4$ case, differentiating the two mentioned main regions of the flow, the attachment line at the leading edge and the lift-up over the top centerline. Comparisons with results of full three-dimensional computations (Gosse *et al.*[41]) of the base flow are currently underway and will be presented elsewhere.

V. Summary and conclusions

A compressible Parabolic Navier-Stokes (PNS) algorithm has been verified and validated in a systematic manner and solutions of the supersonic flows around the circular and elliptic cones are presented. Using this methodology, steady three-dimensional flows with a slow-varying spatial direction can be solved without using a fully three-dimensional spatially evolving DNS and thus saving several orders-of-magnitude of computational effort. The boundary layer solution around a circular cone at zero angle of attack is compared in the incompressible limit with theoretical profiles. Also, the recovered shock wave angle at supersonic conditions is compared with theoretical predictions in the same circular-base cone geometry. Both results show excellent agreement with theoretical predictions. The fully three-dimensional flow field surrounding a 7^0 half minor-axis cone angle elliptic cone of aspect ratio 2 at supersonic regime is presented. The domain is chosen in the way that the shock position and the compressible boundary layer are captured. The two main features of this flow are identified, the attachment line at the leading edge and the lift-up over the top centerline. The crossflow region is also clearly visible in the three-dimensional plots, showing potential crossflow mechanisms of transition.

Acknowledgments

Effort sponsored by the Air Force Office of Scientific Research, Air Force Material Command, USAF, under grant number FA8655-12-1-2004. The U.S Government is authorized to reproduce and distribute reprints for Governmental purpose notwithstanding any copyright notation thereon. The authors would like to thank Dr. Daniel Rodríguez and Dr. Oliver Schmidt for fruitful discussions during the preparation of the newly-developed PNS code solver.

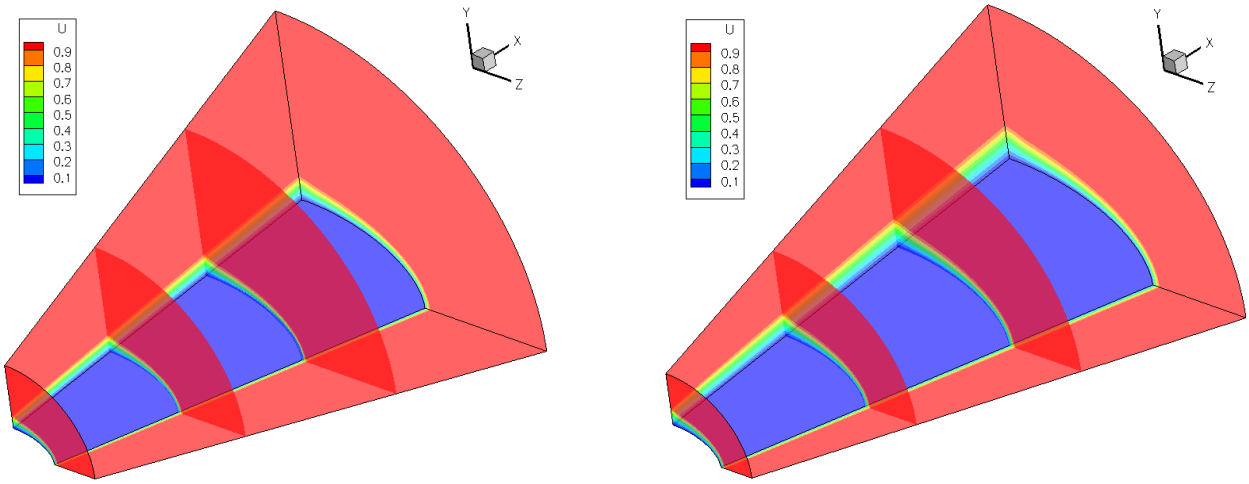

(a) u, $M = 3$

(b) u, $M = 4$

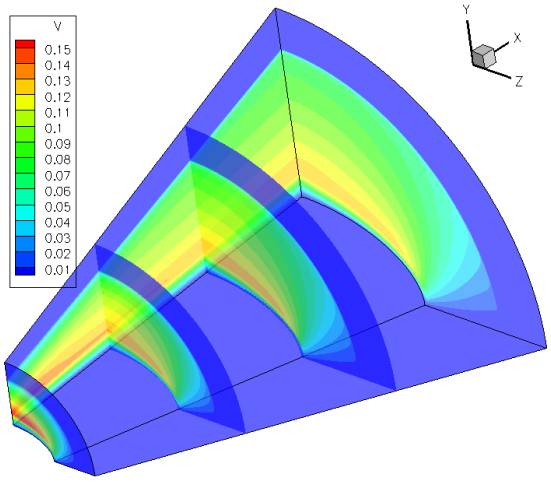

(c) v, $M = 3$

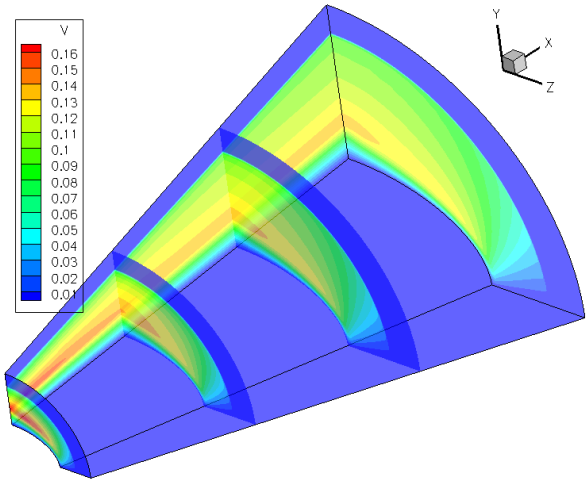

(d) v, $M = 4$

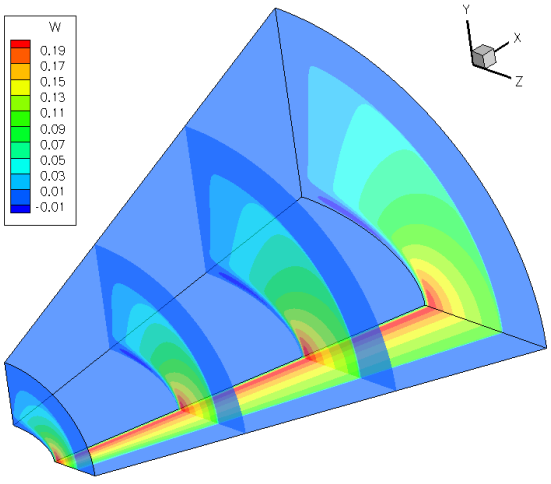

(e) w, $M = 3$

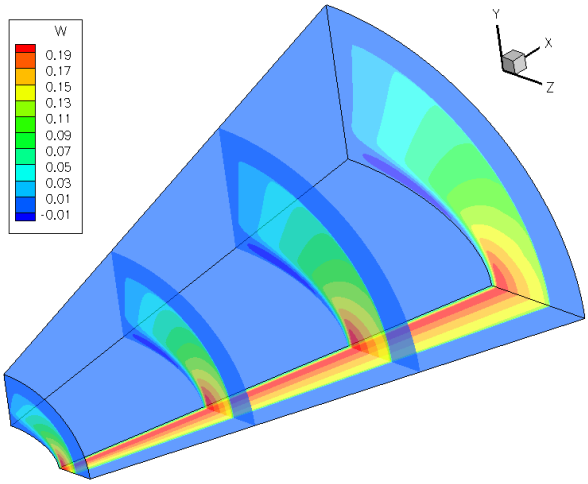

(f) w, $M = 4$

Figure 2. Three velocity components of the flow field from $Re_x = 10^4$ to $Re_x = 3 \times 10^4$ for a 7^0 half minor-axis cone angle elliptic cone of aspect ratio 2 at Mach numbers 3 and 4.

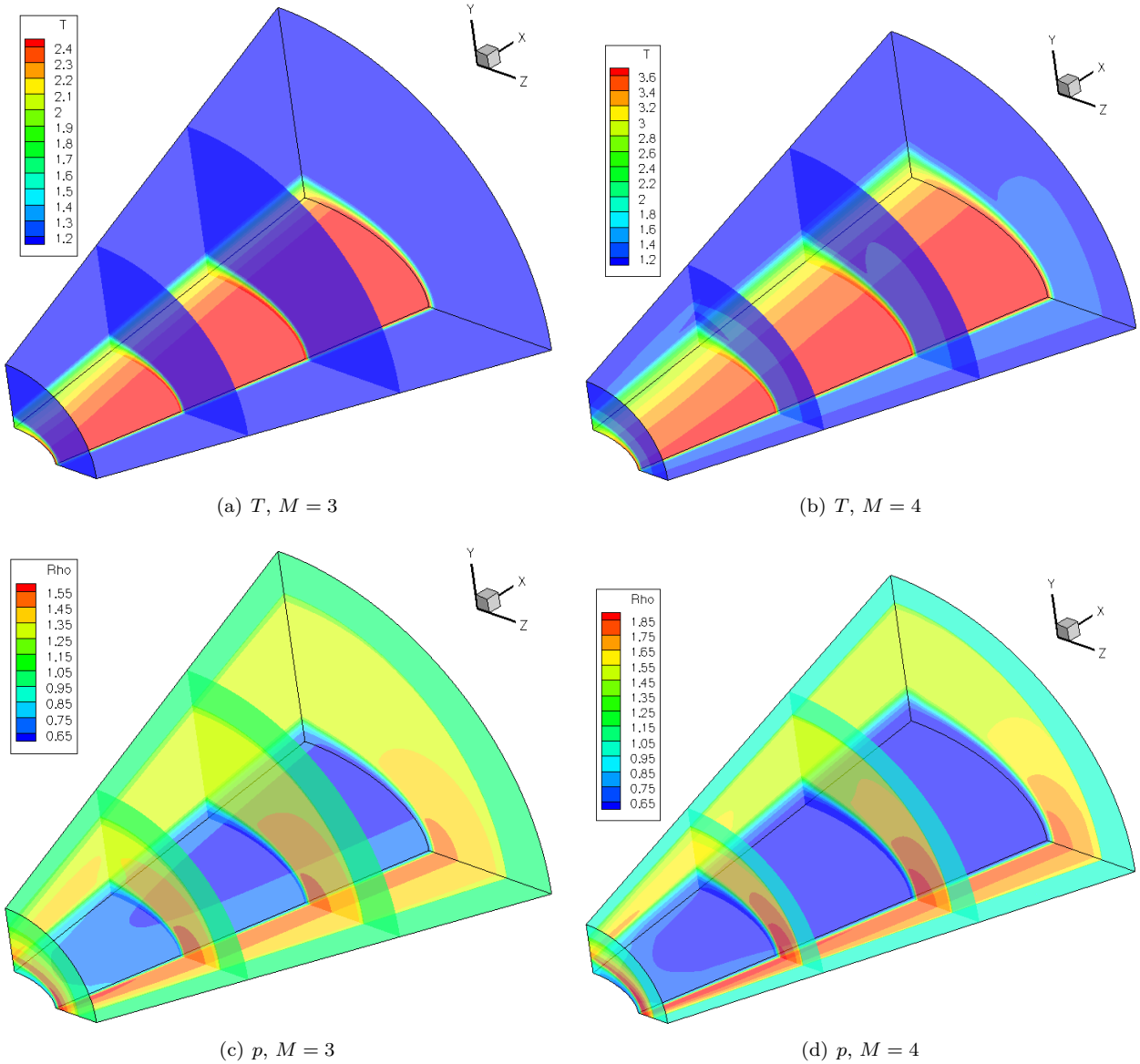

(a) T, $M = 3$

(b) T, $M = 4$

(c) p, $M = 3$

(d) p, $M = 4$

Figure 3. Temperature and density components of the flow field from $Re_x = 10^4$ to $Re_x = 3 \times 10^4$ for a 7^0 half minor-axis cone angle elliptic cone of aspect ratio 2 at Mach numbers 3 and 4.

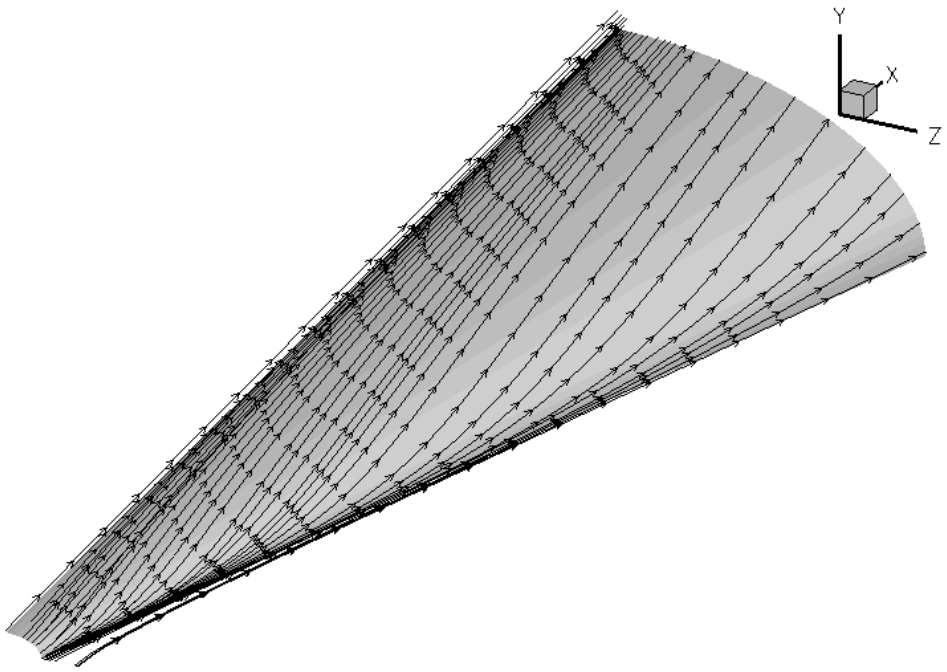

Figure 4. Streamlines near the wall of a 7^0 half minor-axis angle 2:1 elliptic cone at $M = 4$.

References

[1]Schmisseur, J., Schneider, S., and Collicott, S., "Receptivity of the Mach-4 boundary-layer on an elliptic cone to laser-generated localized free stream perturbations," AIAA Paper 98-0532, 1998.

[2]Schmisseur, J., Schneider, S., and Collicott, S., "Response of the Mach-4 boundary layer on an elliptic cone to laser-generated free stream perturbations," AIAA Paper 99-0410, 1999.

[3]Poggie, J. and Kimmel, R., "Traveling instabilities in elliptic cone boundary-layer transition at Ma=8," AIAA Paper 98-0435, 1998.

[4]Huntley, M. and Smits, A., "Transition studies on an elliptic cone in Mach 8 flow using filtered Rayleigh scattering," *European Journal of Mechanics B - Fluids*, Vol. 19, No. 5, 2000, pp. 695–706.

[5]Bartkowicz, M., Subbareddy, P., and Candler, G., "Simulation of boundary layer transition of elliptic cones in hypersonic flow," AIAA Paper 2010-1064, 2010.

[6]Tuckerman, L. and Barkley, D., "Bifurcation analysis for timesteppers," *Numerical methods for bifurcation problems and large-scale dynamical systems*, Springer, 2000, pp. 453–566.

[7]Paredes, P., Theofilis, V., Rodríguez, D., and Tendero, J. A., "The PSE-3D instability analysis methodology for flows depending strongly on two and weakly on the third spatial dimension," AIAA Paper 2011-3752, 2011.

[8]Gómez, F., Le Clainche, S., Paredes, P., Hermanns, M., and Theofilis, V., "Global linear instability at the dawn of its fourth decade: recent progress and remaining challenges," *AIAA J.*, Vol. 50, 2012, pp. 2731–2743.

[9]Bouthier, M., "Stabilité linéaire des écoulements presque paralléles. Partie II. La couche limite de Blasius," *J. Méc*, Vol. 12, 1973, pp. 75–95.

[10]Gaster, M., "On the effects of boundary-layer growth on flow stability," *J. Fluid Mech.*, Vol. 66, 1974, pp. 465–480.

[11]Herbert, T., "Boundary-Layer Transition – Analysis and Prediction Revisited," *AIAA Paper*, Vol. 91, 1991, pp. 0737.

[12]Bertolotti, F. P., Herbert, T., and Spalart, P., "Linear and nonlinear stability of the Blasius boundary layer," *J. Fluid Mech.*, Vol. 242, 1992, pp. 441–474.

[13]Herbert, T., "Parabolized stability equations," *Ann. Rev. Fluid Mech.*, Vol. 29, 1997, pp. 245–283.

[14]Rudman, S. and Rubin, S., "Hypersonic viscous flow over slender bodies with sharp leading edges," *AAIA J.*, Vol. 6, 1968, pp. 1883–1889.

[15]Rubin, S. and Tannehill, J., "Parabolized/Reduced Navier-Stokes Computational Techniques," *Ann. Rev. Fluid Mech.*, Vol. 24, 2004, pp. 117–144.

[16]Tannehill, J., Anderson, D., and Pletcher, R., *Computational Fluid Mechanics and Heat Transfer*, Taylor & Francis, 2nd ed., 1997.

[17]Lin, T. and Rubin, S., "Viscous flow over a cone at moderate incidence-I: Hypersonic tip region," *Comput. Fluids*, Vol. 1, 1973, pp. 37–57.

[18]Lin, T. and Rubin, S., "Viscous flow over a cone at moderate incidence-II: Supersonic boundary layer," *J. Fluid Mech.*, Vol. 59, 1973, pp. 593–620.

[19]Lin, T. and Rubin, S., "Viscous flow over spinning cones at angle of attack," *AIAA J.*, Vol. 12, No. 7, 1974, pp. 975–985.

[20]Helliwell, W. and Lubard, S., "An implicit method for three dimensional viscous flow with application to cones at angle of attack," *Comput. Fluids*, Vol. 3, 1973, pp. 83–101.

[21]Lubard, S. and Helliwell, W., "Calculation of the flow on a cone at high angle of attack," *AIAA J.*, Vol. 11, 1974, pp. 965–974.

[22]Tannehill, J., Venkatapathy, E., and Rakich, J., "Numerical solution of supersonic viscous flow over blunt delta wings," *AIAA J.*, Vol. 20, 1982, pp. 203–210.

[23]Lawrence, S., Chaussee, D., and Tannehill, J., "Application of an upwind algorithm to the three-dimensional parabolized Navier-Stokes equations," *AIAA J.*, Vol. 87, 1987, pp. 1112.

[24]Stuckert, G. and Reed, H., "Linear disturbances in hypersonic, chemically reacting shock layers," *AIAA J.*, Vol. 32, No. 7, 1994, pp. 1384–1393.

[25]Lyttle, I. and Reed, H., "Use of transition correlations for three-dimensional boundary layers within hypersonic flows," AIAA Paper 95-2293, 1995.

[26]Reed, H. and Haynes, T., "Transition correlations in three-dimensional boundary layers," *AIAA J.*, Vol. 32, 1994, pp. 923–929.

[27]Kimmel, R., Klein, M., and Schwoerke, S., "Three-dimensional hypersonic laminar boundary-layer computations for transition experiment design," *J. Spacecraft Rockets*, Vol. 34, No. 4, 1997, pp. 409–415.

[28]Lawrence, S., Tannehill, J., and Chaussee, D., "An upwind algorithm for the parabolized Navier-Stokes equations," *AIAA Paper*, Vol. 86, 1986, pp. 1117.

[29]Stalnaker, J., Nicholson, L., Hanline, D., and McGraw, E., "Improvements to the AFWAL parabolized Navier-Stokes code formulation," U.S. AirForce Wright Aeronautical Labs., TR AFWAL-TR-86-3076, Wright-Patterson AFB, OH, 1986.

[30]Malik, M., "e^{Malik}: A new spatial stability analysis program for transition prediction using the e^N method," Rept. HTC-8902, High Technology Corp., Hampton, VA, 1989.

[31]Hermanns, M. and Hernández, J. A., "Stable high-order finite-difference methods based on non-uniform grid point distributions," *Int. J. Numer. Meth. Fluids*, Vol. 56, 2008, pp. 233–255.

[32]Amestoy, P., Duff, I., Koster, J., and L'Excellent, "A fully asynchronous multifrontal solver using distributed dynamic scheduling," *SIAM Journal of Matrix Analysis and Applications.*, Vol. 1, 2001, pp. 15–41.

[33]Amestoy, P., Guermouche, A., L'Excellent, J.-Y., and Pralet, S., "Hybrid scheduling for the parallel solution of linear systems," *Parallel Computing*, Vol. 2, 2006, pp. 136–156.

[34]Paredes, P., Hermanns, M., Le Clainche, S., and Theofilis, V., "Order 10^4 speedup in global linear instability analysis using matrix formation," *Comput. Meth. Appl. Mech. Eng.*, Vol. 253, 2013, pp. 287–304.

[35]Rodríguez, D. and Theofilis, V., "Massively parallel numerical solution of the BiGlobal linear instability eigenvalue problem using dense linear algebra," *AIAA J.*, Vol. 47, No. 10, 2009, pp. 2449–2459.

[36]Vigneron, Y., Rakich, J., and Tannehill, J., "Calculation of supersonic viscous flow over delta wings with sharp subsonic leading edges," AIAA Paper 78-1337, 1978.

[37]Saad, Y., "SPARSKIT: a basic tool kit for sparse matrix computations, Version 2." 1994.

[38]Mangler, W., "Boundary layers on bodies of revolution in symmetrical flows," Report 45/A/17, Ber. Aerodyn. Versuchsanst. Goett., 1945.

[39]Shapiro, A., *The dynamics and thermodynamics of compressible fluid flow. Vol. 2*, Ronald Press, New York, 1954.

[40]Taylor, G. and Maccoll, J., "The air pressure on a cone moving at high speed," *Proc. R. Soc. London Ser. A*, Vol. 139, 1933, pp. 278–311.

[41]Gosse, R., Kimmel, R., and Johnson, H., "CFD study of the HIFiRE-5 flight experiment," AIAA Paper 2010-4854, 2010.